Conservative and dissipative forces measured by self-oscillator atomic force microscopy at constant-drive amplitude

Vladimir V. Protasenko, Massimiliano Labardi,* and Alan Gallagher
JILA, University of Colorado and National Institute of Standards and Technology, Boulder, Colorado 80309-0440, USA
(Received 19 February 2004; revised manuscript received 17 June 2004; published 10 December 2004)

The fundamental-mode oscillation of an atomic force microscope cantilever, operated in the self-oscillator (SO) mode, is analyzed to interpret resonant frequency (f_r) and oscillation amplitude (A) in terms of probe-sample conservative and dissipative forces. Measurements of f_r and A versus probe-surface gap, for a H-terminated silicon probe and surface in air, have been carried out in the constant-excitation (CE), SO mode for a variety of SO phases. We provide the full z dependence of A and Δf due to both conservative and dissipative forces, evidencing a minimum value of tip-sample closest approach distance expected from theory. The existence of such a minimum preserves tips from destructive interaction in CE mode.

DOI: 10.1103/PhysRevB.70.245414 PACS number(s): 68.37.Ps, 81.40.Jj, 07.79.Lh

I. INTRODUCTION

Dynamic force spectroscopy (DFS) is a scanning probe microscopy technique that is capable of measuring the local interaction potential between a surface and the apex atoms of an atomic force microscope (AFM) probe. This spectroscopy, which is utilized here, can provide information on the energy dissipation due to the dynamical interaction of the atoms in close contact.

Atomic force microscopy[1] in the noncontact mode[2] is performed by oscillating a sharp-tipped probe mounted on a cantilever, in the z direction normal to the sample surface, at frequency f. This is usually done by periodically displacing the cantilever base (sketched in Fig. 1, "OPCS") with a piezoactuator slab, and the probe motion is typically detected by the optical lever method.[3] If the tip interacts with an external force field, as occurs in proximity to a surface, the oscillatory motion will be altered by the interaction. This provides a basis for maintaining a constant probe-surface gap during scanning, as well as information on the conservative and dissipative interactions between the probe and surface.

When the tip oscillation is excited by a constant-frequency, constant-drive amplitude (A_d) motion of the cantilever base, this is referred to as *noncontact mode* when the oscillation amplitude (A) of the tip is below $\sim$2 nm and smaller than the probe-surface gap.[2] For higher amplitudes (ten to hundreds of nm) it is named *intermittent-contact mode* or *tapping mode*.[4] For a given lever stiffness k, increasing the oscillation amplitude permits a closer approach distance before jump-into-contact at z_{JIC}, since $F_{TS}(z_{JIC})=kA$, where F_{TS} is the tip/sample interaction force.[5] With standard values of k for microfabricated cantilevers (1–100 N/m) and sufficient amplitude, the entire attractive and repulsive regions of interaction can be studied without loss of oscillation. A measurement of oscillation phase ϕ, relative to the excitation, is named phase imaging,[6] and can provide quantitative information on the local surface dissipation.[7]

An alternate to phase imaging is the *self-oscillator* (SO) technique,[8] in which instead of using a fixed drive frequency, the cantilever becomes the frequency-selecting element in a self-oscillator circuit. This is achieved by positive feedback of the lever-deflection signal to the cantilever-base piezo, with the feedback circuit maintaining a constant ϕ. Maximum oscillation amplitude occurs at $\phi=\pi/2$ that defines the resonance frequency f_r, with $\pi/2<\phi<\pi$ above resonance and $0<\phi<\pi/2$ below. If the resonance width does not change or $\phi=\pi/2$, the cantilever oscillation frequency instantaneously follows changes in f_r as it varies due to external forces. The frequency shift ($\Delta f_r=f_r-f_0$, where f_0 is the free-lever resonance) due to the probe/sample interaction is measured with a frequency-to-voltage converter, and this can be fed back to maintain the probe-surface gap during scanning. For DFS measurements, the importance of using the

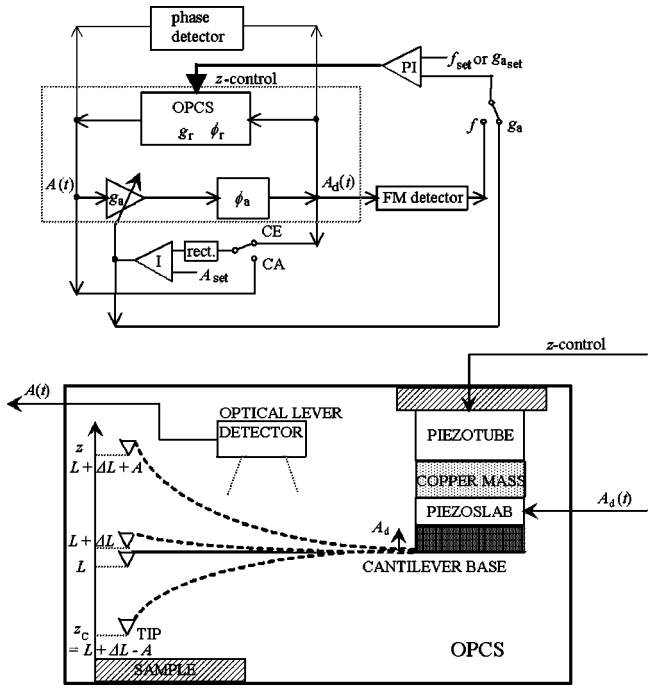

FIG. 1. Sketch of the experimental setup (top). The dashed box delimits the self-oscillator section. I=integral controller of oscillation amplitude; rect=rectifier; PI=proportional-integral controller of z-position; OPCS=oscillating probe/cantilever system, sketched separately on bottom (proportions are not respected).

SO mode, versus the fixed-f mode, resides mainly in faster response, more straightforward DFS interpretation, and improved operation and approach stability.

Two different operation modes are commonly employed in the SO method; the *constant-amplitude* (CA) *mode*[8] and the *constant-excitation* (CE) *mode*.[9] In the CA mode, A is held constant by an automatic gain control (AGC) feedback loop that controls the driving amplitude A_d of the piezoslab.[8] The response time is not limited by the Q factor of the cantilever oscillation in this mode, so it is particularly useful in vacuum. Information about dissipation may be extracted from the AGC feedback signal g_a, which represents A_d/A.[10] In the CE mode, the AGC circuit maintains A_d at a constant value, while A is allowed to vary. The amplitude response time is Q-limited in the CE mode, so that it is most useful in air. However, the CE mode has a significant advantage compared to CA mode, as has been previously pointed out.[9] It tends to preserve the probe tip from damage, saving experimental time and yielding reproducible measurements. In addition, as shown below, it is free of approach or scan instabilities at the A values used for DFS, making it convenient compared also to tapping mode.

Theoretical studies and numerical simulations have predicted the effect of conservative and dissipative forces on A and Δf in the CE mode,[11,12] with $\phi=\pi/2$, mainly as an extension of the established knowledge of the CA mode.[13] Here we extend the analysis to all ϕ values, and calculate the expected dependence of A and Δf on the closest approach distance z_c for model interactions. We provide experimental A and Δf versus L and ϕ, in the CE mode in ambient air, and reduce these to functions of z_c. Comparing to the model interactions then provides the conservative and dissipative forces acting on the lever. In our approach-curves, for various ϕ, we always observe a minimum z_c versus L, and therefore a maximum interaction strength that is anticipated by the theory. This explains the protection of the probe obtained experimentally in CE mode, thereby leading to high reproducibility and low time consumption in experiments.

The paper is organized as follows: In Sec. II the experimental arrangement is described, along with a brief review of the SO method useful for better understanding of phase-locked, SO principle; next, approach curve data of H-terminated silicon tips on silicon surfaces with CE, SO mode operation in air are presented. In Sec. III, starting from the accepted models that relate oscillation amplitude and frequency shift to the conservative and dissipative forces, relevant relations are carried out for the generic SO phase, in order to allow interpretation of our data. Based on those relations, A and Δf are calculated for an example pair of conservative and dissipative forces, in order to fit our experimental curves and characterize the operation of our tip/sample system in ambient air. Finally, in Sec. IV we summarize our findings.

II. MEASUREMENTS IN CE, SO MODE

A. Experimental setup

Experiments have been conducted with a home-made, dynamic-mode AFM described elsewhere[14] and operated as in Fig. 1. The microscope is operated in the SO mode with adjustable feedback phase (ϕ_a). The cantilever is the frequency-selective element in a positive feedback loop, depicted in Fig. 1 with the dashed box and composed of an adjustable-gain amplifier, a phase shifter, and the excitation/detection system of the cantilever motion, named an oscillating probe/cantilever system (OPCS). The OPCS contains the cantilever, with base mounted to a small, high-frequency piezodriver, then to a copper mass and a tube piezoactuator for z-control. A laser and split-diode detector measures the deflection angle of the probe end. Additionally, an AGC circuit detects the oscillation signal amplitude and adjusts the system gain by means of a negative-feedback loop to stabilize it to a set value (A_{set}). When the "CA/CE" switch in Fig. 1 is in the "CA" position, the lever oscillation is rectified, A is held constant, and the system is in the CA mode. With the switch in the "CE" position, A_d is detected and stabilized, and the constant-excitation mode is obtained. A frequency modulation (FM) detector provides a signal proportional to f, which may be utilized for DFS as well as for distance regulation (z-control in Fig. 1) when the switch on the right side of Fig. 1 is in the "f" position. Alternatively, with the switch in the "g_a" position the value of g_a is used for z-control. This yields to constant A *and* A_d scans with constant dissipation power.

The approach curves are recorded as follows. In CE mode and with a fixed $\phi_a=\phi_{set}$, the sample is approached with A-feedback until stabilized at amplitude A_{set}, typically with $A_{set}\cong 0.9\ A_0$ and free-lever amplitude $A_0\cong 30$ nm. The A-feedback is then disconnected, the tip is withdrawn a fixed distance, next moved slowly forward to beyond the setpoint, then withdrawn slowly, and finally returned to A-feedback at A_{set}. The acquired signals for each ϕ_a are $\Delta f(L)$ and the AGC control voltage $[V_{AGC}(L)]$, where L is the probe-sample gap for an undeflected lever (Fig. 1). The SO feedback is still active and the AGC maintains a constant A_d during this approach and withdrawal, by variable-gain amplification of the lever-reflection optical signal. Thus, AGC gain (g_a) is proportional to A_d/A, and is a measured function of V_{AGC} (we calibrate g_a versus V_{AGC} using an external signal generator), so this provides $A(L)=A_d/g_a(L)$.

With the tip withdrawn, varying the phase in the SO mode yields $A(f)$, the cantilever resonance curve. The phase is independently measured by a home-made, high-frequency lock-in amplifier. As expected, this curve matches the resonance curve obtained by exciting the cantilever with an external function generator [Eq. (6), see Sec. III], so it is not shown. This indicates that the SO cantilever excitation provides the same behavior as monochromatic excitation, and that no spurious modes within the support structure are excited. For our AFM levers in air, this curve typically fits $Q=200-280$.

The silicon probe and sample were alcohol-cleaned and H-terminated in buffered hydrofloric acid, an hour or so before taking the data. They are also both n-doped and held at fixed potential difference, generally 0 V, unless stated otherwise. The mounted probe and sample are exposed to an ionized Ar flux to eliminate static charges before measurements.

B. Distance calibrations

The main reduction performed on the Δf and A data is from functions of L to functions of "closest approach dis-

tance" $z_c(L)=L-A(L)+\Delta L[A(L),f(L)]$, where L is obtained from the z-distance piezovoltage (V_Z) and A from the AGC control voltage (V_{AGC}), as described above. Due to the cycle-averaged force on the lever, it oscillates about a shifted z location, $L+\Delta L$, with ΔL given by Eq. (10) of Sec. III in terms of A and Δf. ΔL is usually a small z correction in the attractive (negative Δf) region, but is important in the strongly repulsive region. z_c is the minimum tip-sample distance reached during the oscillation; since only z_c displacements are meaningful, we normally set z_c to zero at its smallest value within a set of approach curves.

Since Δz_c during approach is primarily the difference between two larger numbers, ΔL and ΔA, and the surface interaction occurs within a small Δz_c range, accurate calibration of ΔL and A (in absolute units, e.g., in nanometers) is essential. We utilize several techniques to calibrate the piezotube expansion coefficient $\Delta L/\Delta V_Z$. We measure $\Delta L/\Delta V_Z$ interferometrically and by scanning a calibrated lithographic-Si sample with 22 nm step height. These agree within 5%, the typical variation due to hysteresis. To obtain the calibration factor between A and S_{PD}, the ac signal on the split photodetector, the ac signal/dc signal combined with the laser-reflection geometry and deflected-lever shape may be considered. However, a more accurate determination of A/S_{PD} (in nm/V) is obtained by changing the cantilever amplitude by ΔA and measuring the corresponding ΔL while the microscope is operating in z-feedback. This is done in the repulsive regime, (positive Δf), since z_c is then almost independent of A. For example, if S_{PD} is decreased by 30% and $\Delta L=30$ nm maintains the fixed Δf, then $\Delta A=30$ nm occurred to maintain the constant z_c, and the original A value was 100 nm. This accuracy of this calibration is also limited to ~5% by hysteresis in z-piezotube motion, which is apparent in forward versus backward z scans. For this reason, the approach data were taken with large forward scans, yielding a fairly reproducible and linear relation between L and V_Z, but still several percent variations occur depending on the previous z-piezo motion. Varying either calibration by 5% in the reduction of $A(L)$ data to $A(z_c)$ yields quite different z_c ranges for the surface interaction, while adjusting one calibration within this 5% range yields $A(z_c)$ and $\Delta f(z_c)$, which look appropriate based on our theoretical expectations. Clearly, this does not allow us to accurately establish the steepness of the conservative and dissipative forces from our current data. Accurate, hysteresis-free motion transducers are available, and in hindsight this is a crucial component for accurate CE dynamic force microscopy.

C. Results

1. Approach curves

With the freely oscillating cantilever, we could adjust the SO feedback phase ϕ_{set} within 40° either side of the 90° that yields f_r. We confirmed that, for the entire positive feedback loop, the phase variation with Δf and Δg_a was negligible; all phase/frequency dependence was due to the lever mechanical resonance. Operation at all ϕ_{set} seemed affected by the same fluctuation and noise, at least in the steady state (as also apparent from Ref. 15, Fig. 1). Figure 2(a) shows measured

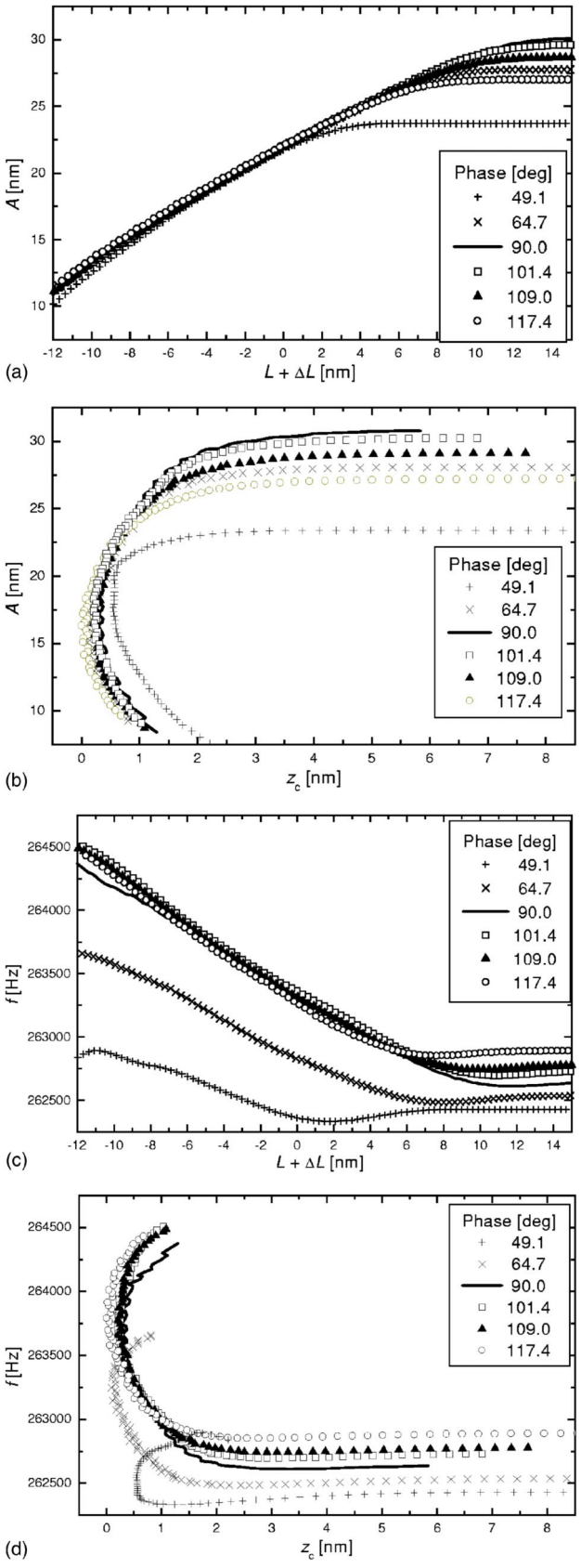

FIG. 2. Experimental approach curves for amplitude [(a),(b)] and frequency [(c),(d)], plotted either vs $L+\Delta L$ [(a),(c)] and vs z_c [(b),(d)]. Different amplifier phases ϕ_a were used.

A versus L, for a range of ϕ_{set}. For much of the approach data, $\Delta\phi_a < 0.1°$ was observed, but occasionally $\Delta\phi_a$ on the order of 0.5° occurred, with the change more pronounced for ϕ_a below 90° (−0.14° at $\phi_a = 117.4°$ and −0.6° at $\phi_a = 49.1°$). Figure 2(b) shows the same data versus the closest approach z_c, obtained as previously described. (The data versus L are smoothed by adjacent-averaging over a range of ±0.5 nm.) It is evident that a minimum z_c exists, with a reversal as L is further decreased. Reproducible z-approach and imaging measurements, including sharp images of nanometer-sized quantum dots, were obtained over an extended time period for each probe. This confirms that this mode preserved the tips from damage, and probably also from loss of the H-termination by hard contact with the surface. In contrast, tip damage is often observed during atomic resolution imaging using the CA mode, even under UHV conditions where less lever dissipation occurs.[5,16]

In Figs. 2(c) and 2(d), Δf is plotted versus L and z_c for the ϕ_{set} values in Figs. 2(a) and 2(b); the A and Δf data were obtained simultaneously. Note that, as mentioned below [Eq. (14), Sec. III], A is only slightly less than A_0 at the minimum of Δf. From Fig. 2(b), it is evident how all curves group into the same one in the repulsive region close to the minimum z_c. Note that, for ϕ_a near $\pi/2$, $A \cong A_0/2$ at the minimum z_c, as predicted theoretically (Sec. III). Also note that, except for the $\phi_a = 49°$ case, Δf monotonically increases in the repulsive region in Fig. 2(d), even though z_c reverses direction. Thus, if positive-Δf feedback was used, the tip would normally be protected, as in the case of A-feedback.

In SO mode with $\phi_a = \pi/2$, any amplitude change is entirely due to surface-induced dissipation, and Δf is entirely determined by the conservative forces. At other ϕ_a, increased damping also influences Δf, since an "effective Q" change is induced [see Eq. (5), Sec. III]. Indeed, the amplitude versus separation curves [Figs. 2(a) and 2(b)] are less dependent on ϕ_a than the frequency shifts [Figs. 2(c) and 2(d)].

2. Voltage dependence

The dependence of $\Delta f(z_c)$ and $A(z_c)$ on probe bias (V_P) was measured for −5 to +5 V bias. If we define the z_c location of minimum Δf_r as $z_m = 4$ nm, then for $V_P = 0$ we observed $\Delta f_r \cong 0$ for $z_c > 7$ nm. Applying bias, for $z_c > 7$ nm, we measured $\Delta f \cong C_V(\mathrm{nm}/z)^m[(V_P - V_{offset})/\mathrm{V}]^2$, with $|V_{offset}| < 1$ V and typically $m \sim 0.5$ and $C_V \sim 3$ Hz. For $z_c < 6$ nm, an additional close-range increase in Δf occurred, often with some asymmetry versus $V_P - V_{offset}$. Transmission electron microscope (TEM) images of one of these probes, after use, showed a very smooth and perfect ~50-nm-radius hemispherical tip. This clearly indicated melting during gentle contact with the applied voltage. The probe and sample are similarly doped, n-type silicon, cleaned by HF etch, so no offset is expected. $A(z_c > 7$ nm) increased with $|V_P|$ for one probe, but was essentially constant with several others. Note that an A increase before the repulsive regime in the CE mode has been also previously reported in Ref. 9.

One can estimate the expected dissipation due to the capacitive current through the tip apex. The capacitive charge ($q = CV$) oscillating on the probe tip and substrate should dissipate, within the spreading resistance $R = \rho/d$, an energy $E_C \sim Rq^2/\Delta t$ in one cycle, where $\Delta t \sim 0.1$ μs is the interaction time, $\rho \sim 0.01\ \Omega$ cm is the silicon resistivity, $d \sim 10$ nm is the capacitor diameter, and $C = 4\pi\varepsilon_0 d^2/z_c = 10^{-17}$ F for $z_c = 1$ nm. This yields $E_C \sim 10^{-3}$ eV at 3 V bias, compared to the estimated free-lever dissipation of 2500 eV. Thus, we do not expect the lever amplitude to decrease significantly through such dissipation.

III. MODEL

A. Theory

A theoretical description of the CE mode has been given in Refs. 11 and 12. In order to emphasize certain features of the motion, and to allow for arbitrary ϕ_a, we summarize the fundamental-mode theory here. We also generalize to CA and fixed-f modes, to allow comparative analysis between modes with a consistent notation.

The AFM lever deflection is taken as $\Delta L + A\cos(\omega t)$, the surface-probe separation is $z(t)$ (see Fig. 1), a conservative surface-probe force $F_{cons}(z)$ and a dissipative force $F_{diss}(z, dz/dt)$ act on the lever, and $(2\pi f_0)^2 = \omega_0{}^2 = k/m^*$, with k the lever spring constant and m^* an effective mass that yields the free cantilever resonant frequency f_0. Solution of the equation of motion of the AFM lever is available from the literature,[11,12] although here we do consider the solution for a generic phase, and insert the average bending ΔL for more accurate definition of z_c. Here only fundamental-mode components of the interactions are included: $F_{1,cons} = (\omega/\pi)\int F(t)_{cons}\cos(\omega t)\mathrm{d}t$ and $F_{1,diss} = (\omega/\pi)\int F(t)_{diss}\sin(\omega t)\mathrm{d}t$, where the integrals are over one cycle and the t dependence comes from $z(t) = L + \Delta L - A\cos\omega t$. Thus, $F_{1,cons}$ and $F_{1,diss}$ are functions of the closest approach distance, $z_c \cong L + \Delta L - A$. With the approximations $|f - f_0|/f_0 \ll 1$, $1 - f^2/f_0{}^2 \cong -2(f - f_0)/f_0$, the fundamental-mode solution has a resonant frequency

$$f_r = f_0(1 - F_{1,cons}/2kA), \tag{1}$$

and an effective Q

$$1/Q_{eff} = (1/Q + F_{1,diss}/kA), \tag{2}$$

to yield

$$\tan\phi = f_0/2Q_{eff}(f - f_r) \tag{3}$$

and

$$A_d^2/A^2 = 4[(f - f_r)/f_0]^2 + [1/Q_{eff}]^2. \tag{4}$$

Equations (3) and (4) describe the fundamental-mode phase and amplitude with surface forces, and with $f_r \to f_0$ and $Q_{eff} \to Q$ they describe the freely oscillating lever. As in Ref. 17, one can express f_r as a function of L and A, and invert Eq. (4) to obtain f versus L, A and $A_d = QA_0$, where A_0 is the free-lever amplitude:

$$\begin{aligned} f &= f_r(A,L) \pm f_0[A_d^2/A^2 - 1/Q_{eff}(A,L)^2]^{1/2}/2 \\ &= f_r(A,L) + f_0\cot\phi/2Q_{eff}(A,L), \end{aligned} \tag{5}$$

where we have made explicit the dependence of f_r and Q_{eff} on A and L. Equation (5) generalizes Eq. (4) of Ref. 17 to include dissipative forces. Combining Eqs. (3) and (4) yields

$$\sin^2 \phi(A,L) = [A/A_d Q_{eff}(A,L)]^2, \quad (6)$$

where $g_a = A/A_d$ is also a function of A and L. Since $Q_{eff} = Q$ in the absence of a surface dissipative force, Eq. (6) shows that A/A_d is uniquely related to ϕ if $F_{diss}(t) = 0$, even when a conservative force changes the resonance frequency. Equation (6) can be used to experimentally establish $Q_{eff}(L,A)$, and thus $F_{1,diss}(A,L)$, from ϕ and A/A_d versus A and L. In the SO method, ϕ is locked by the oscillator circuit and is constant, so any variation in A/A_d is entirely due to $F_{1,diss}$. A measurement of $f_r(A,L)$, and hence of $F_{1,cons}(A,L)$, is most easily done by measuring f versus A and L with $\phi = \pi/2$, since in this case $f = f_r$.

In this fundamental-mode analysis, Eq. (1) shows that f_r is only influenced by the conservative force, even though the probe/surface interaction is concentrated in a small fraction of the cycle. The lever emerges from this interaction with total energy decreased by E_{diss}, and this energy is gradually recovered during the remainder of the cycle. The energy just before surface interaction is $E_{diss}/2$ above the average, speeding up the cycle, just after the interaction it is $E_{diss}/2$ below the average, slowing down the cycle, while E_{diss} is gradually recovered during the remainder of the cycle. These are compensating effects and there is no net fundamental-mode frequency shift due to the dissipative energy loss.

It is also well known, from fixed-f theoretical developments,[18] that the energy relation between probe-sample dissipated energy per cycle (E_{diss}) and oscillation amplitude is

$$E_{diss}/E_0 = y y_d - y^2, \quad (7)$$

where $y = A/A_0$, $y_d = A_d/A_{d0}$, A_0 is the free-lever amplitude, A_{d0} is the free-lever base amplitude, $E_0 = \pi k A_0^2/Q$ is the free-lever dissipation, and $E_{damp} = \pi k A^2/Q$ the actual lever dissipation per cycle. We note that E_{diss} equals the lever velocity $[A\omega \sin(\omega t)]$ times $F_{diss}(t)$, integrated through a surface interaction, so that $E_{diss} = \pi A F_{1,diss}$. Using this in Eqs. (2) and (6) also yields Eq. (7). E_{diss} will normally be a function of A as well as the force, as will be evident in our example below [Eq. (14)]. In CE mode, $y_d = 1$ in Eq. (7), and inversion of this equation yields

$$y = [1 \pm (1 - 4E_{diss}/E_0)^{1/2}]/2. \quad (8)$$

As L decreases from ∞ in CE mode, the positive sign applies in Eq. (8), z_c decreases, E_{diss} increases, and A decreases toward $A_0/2$, where $E_{diss} = E_0/4$. When $A < A_0/2$ $\left(y < \frac{1}{2}\right)$, the negative sign applies to further decreases in L. This L decrease is accompanied by A decreasing faster than L, so that z_c increases and E_{diss} decreases. Thus, for $y < \frac{1}{2}$, the probe/surface interaction weakens as the cantilever base moves closer to the surface, and the maximum E_{diss} is $E_0/4$. This tends to protect the probe from damage, although the time to come to this equilibrium condition is $\sim Q/\omega$ and this does not protect against a rapid decrease in L.

B. Description of CA and fixed-f modes

In the CA mode, where A is held constant and A_d is varied, Eq. (7) becomes

$$E_{diss} = E_0[y_d - 1]. \quad (9)$$

Here oscillation is sustained even when a large E_{diss} occurs in each surface collision, and as a result a larger range of E_{diss} can be studied. For the same reason, it is much easier to damage the probe tip in this operating mode, particularly in air where E_0 is large.

In CE mode $y = Q_{eff}/Q$, while in CA mode $1/y_d = Q_{eff}/Q$, and in both cases $Q/Q_{eff} = 1 + QF_{1,diss}(z_c,A)/kA = 1 + E_{diss}(z_c,A)/E_{damp}$. From Eq. (1), comparing the definition of $F_{1,cons}$ to the cycle-averaged conservative force, and equating this to k times the average lever deflection (ΔL), one obtains

$$\Delta L = A\Delta f/f_0. \quad (10)$$

This allows ΔL to be easily established from experimentally measured quantities, for use in $z_c = L - A + \Delta L$, although in the present experiment $\Delta L < 0.2$ nm due to limiting the size of the repulsive interaction and this is not a very important correction to $z_c \cong L - A$.

Combining Eqs. (2) and (5) yields

$$f(z_c,A,\phi) = f_r(z_c,A) - (f_0/2Q)[1 + QF_{1,diss}(z_c,A)/kA]\cot\phi, \quad (11)$$

where $f_r(z_c,A)$ is given by Eq. (1). $F_{1,diss}(z_c,A)$ can also be expressed in terms of average power dissipation, $P_{diss}(z_c,A) = f_0 E_{diss}(z_c,A) = \pi f_0 A F_{1,diss}(z_c,A)$, and the substitution $1 + QF_{1,diss}(z_c,A)/kA = 1 + (1/y^2)E_{diss}(z_c,A)/E_0$ is useful, particularly in the CA mode where $y = 1$. Thus, the ϕ dependence of $f - f_0$ with fixed A results from the Q change caused by the dissipative energy loss. The ϕ dependence of A/A_d is given by Eq. (6), with Q_{eff} a function of A and z_c.

Finally, for describing the constant frequency and excitation mode (fixed-f mode or tapping mode), where phase is not controlled, it is useful to combine the first part of Eq. (5) with Eq. (7) to obtain $f(A_0,L)$ as

$$f = f_r(A,L) \pm (\pi f_0/Q)[(1/y^2) - (1 + y - y^2)^2]^{1/2}/2. \quad (12)$$

This describes operation with a dissipative force, while replacing the factor $1 + y - y^2$ with 1 describes purely conservative forces.

C. Experimental implications

It bears repeating that no fundamental-mode A changes occur in SO mode for entirely conservative interactions, for any ϕ_{set}, but dissipation normally plays a major role and causes A/A_d to vary. In the CE mode, A is observed to decrease monotonically with decreasing L. As shown previously, in the CE mode the maximum power dissipation due to a dissipative surface interaction is $\sim$25% of the free-lever dissipation, and this occurs when A is $\sim$50% of the free-lever amplitude. This limits the maximum indentation of the tip and the strength of the interaction, so that A can be used safely for distance stabilization during scanning.

We see in Eq. (1) that in SO mode the resonance frequency f_r depends only on the conservative force, and from Eq. (6) $g_a = A_d/A$ depends only on the dissipative force, re-

gardless of the chosen phase. Thus, in the SO mode, *gain adjustment will occur exclusively in presence of dissipation, for any value of phase*. As has been generally recognized, in the SO mode Δf *is entirely determined by the conservative force only for* $\phi_a = \pi/2$. Equations (1) and (2) show that Δf reflects the fundamental-mode component of this conservative force, versus the closest approach distance, $z_c = L + \Delta L - A$. Equation (9) shows that in the CA, SO mode, g_a responds to the dissipated energy/dissipative force versus z_c, independent of the conservative force. Equations (7) and (8) show that g_a similarly provides the dissipated energy versus z_c in the CE mode, again without influence of the conservative force. Thus, quantitative interpretation of DFS data taken in CE mode contains no additional difficulty with respect to the more established CA mode, while it is still simpler than the fixed-f mode. Therefore, in some sense, the CE mode of the SO method maintains many of the advantages of tapping mode, while its employment in DFS is less likely to damage probes than CA mode.

D. Example with model potential

We will now apply the equations describing the SO mode and analyzed above to attempt a fit of our experimental curves. We calculate here f_r and A/A_d in the SO mode for an example set of conservative and dissipative probe/surface forces, $F_{cons}(z)$ and $F_{diss}(z)$, relevant to our system. The perturbations to sinusoidal lever motion are very small, so that a superposition principle holds; the conservative and dissipative forces can be expressed as a sum of terms, and each term yields a frequency shift or energy loss versus z_c that is independent of the other terms. The data presented in Sec. III yield a negative $\Delta f_r(z_c)$ that greatly exceeds that due to the Van der Waals attraction, and has a much shorter range. At smaller z_c a positive Δf_r occurs due to the strongly repulsive interaction. To match the typical $\Delta f_r(z_c)$ behavior of the data, we use a conservative force of the form $F_{cons}(z) = C_{cons}\{-M \exp[-(z-z_m)/s] + M^{1/2} \exp[-M(z-z_m)/s]\}$, where C_{cons}, M, z_m, and s are parameters of the potential. An analytic approximation for the solution of the equation of motion using the expansion $x(t) = A\cos[2\pi ft + \phi(t)]$, where $x(t)$ is the probe position, and $A \gg s$ yields:

$$\Delta f_r(z_C) = \frac{C_{cons} s^{1/2} f_0}{2(2\pi)^{1/2} k A^{3/2}} \{-M \exp[-(z_C - z_m)/s] + \exp[-M(z_C - z_m)/s]\}, \quad (13)$$

where f_0 is the lever resonant frequency. As will be shown below, with $M = 1.1$, $s = 1$ nm, $C_{cons} = 100$ nN, and any value for z_m (the minimum of Δf_r), this yields the typically observed negative $\Delta f(z_c)$.

For the dissipative force we choose a power law times the probe velocity: $F_{diss}(z, dz/dt) = C_{diss} dz/dt (z_m/z)^n$. Again expanding $x(t)$ as $A\cos[2\pi ft + \phi(t)]$, and keeping leading terms, yields an analytic lever energy loss per cycle (E_{diss}). For an exponential force this approximation agrees with a previous result,[19] but in the present case a power law with $n \cong 6$ better represents the steepening of the measured $E_{diss}(z_c)$ and the relation between Δf and E_{diss}. Note that a sum of exponentials works as well, but using the power law yields an analytic expression for $z_c(A)$. This yields, for $A \gg z_m/n$,

$$E_{diss} = 8\pi f_0 C_{diss} A^{1/2} z_m^{1.5} n^{-1.6} (z_m/z_c)^{n-1.5}, \quad (14)$$

where we have used an approximation valid for $n \geqslant 6$: $\int x^2(1+x^2)^{-n} dx = 0.7n^{-1.6}$. To roughly fit the data, we take $n = 6$ and $z_m = 4$ nm, and use the same z_m in Eq. (13). For $A = 30$ nm the data typically yield $E_{diss} \cong 50$ eV and $\Delta f_r \cong -80$ Hz at z_m. To obtain this from Eq. (14) we take $C_{diss} = 3 \times 10^{-6} (\text{nm}/z_m)^{1.5}$ kg/s for a typical lever, characterized by $k = 40$ N/m, $Q = 280$, and $f_0 = 2.7 \times 10^5$ Hz. The free-lever dissipation, $E_0 = \pi k A_0^2 / Q \cong 2500$ eV, greatly exceeds $E_{diss}(z_m)$, so $A \cong A_0$ at z_m.

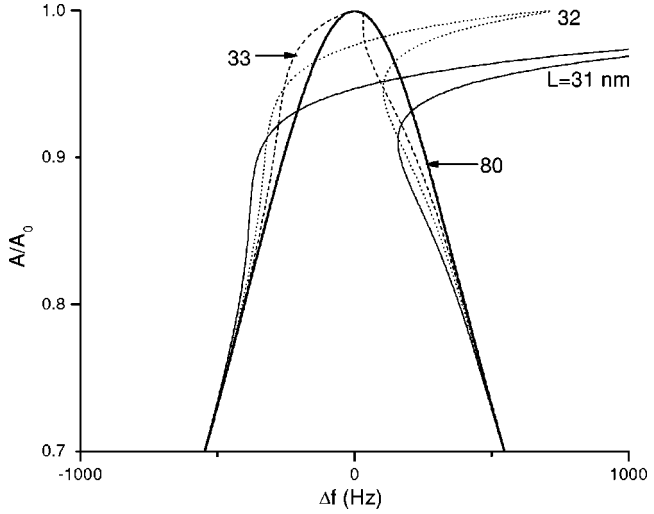

FIG. 3. Calculated oscillation amplitude (A) as a fraction of free-lever amplitude on resonance (A_0), versus frequency offset from lever resonance (Δf) and the average probe-surface separation (L). The example conditions are $A_0 = 30$ nm, $f_r = 300$ kHz, and the conservative force used in Eq. (13), which is minimum at $z = 4$ nm. Note that the probe's closest approaches are 1, 2 and 3 nm for $A/A_0 = 1$ and $L = 31$, 32, and 33 nm, respectively.

Figure 3 shows resonance curves in CE mode calculated for several L values and the above assumed forces. These $A(f)$ curves are calculated by using Eq. (13) for f_r in Eq. (12), and taking $z_c = L - A$ and $z_m = 4$ nm. This shows the $F_{diss} = 0$ case; the dissipative form of Eq. (12), obtained by means of Eq. (14), yields a similar plot, but with a 10%–20% wider half-height width due to the lower Q_{eff}. The peak amplitude occurs on resonance, with $A(f_r) = A_0 = QA_d$ and $\phi = \pi/2$. As was pointed out above, the double-valued character of $A(f)$ can lead to instabilities in fixed-f mode. However, since each A/A_0 value and branch corresponds to a unique phase, there is no instability in SO mode. This is consistent with Eq. (6), where the phase depends only on A/A_d, or equivalently A/A_0, independent of the value of f_r. Thus, with ϕ_a constant during approach in SO mode, A is constant if $F_{diss} = 0$, and g_a increases smoothly (without instability) during approach in the CE, SO mode with $F_{diss} \neq 0$.

The $\Delta f(z_c)$ and $E_{diss}(z_c)$ that result from Eqs. (13) and (14) are shown in Figs. 4 and 5 for the CA mode and examples of

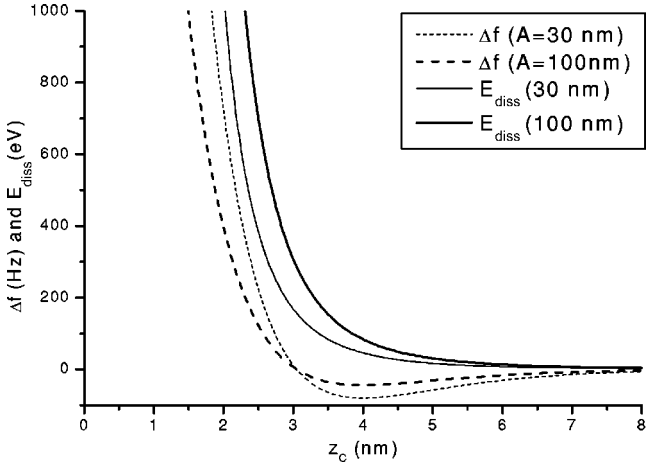

FIG. 4. Calculated angular frequency shift and dissipative energy loss versus z_c, the probe-surface gap, for CA operation and the forces described in Sec. III. The lever-damping energy loss per cycle (E_0) equals 2500 (28 000) eV for $A=30$ (100) nm.

$A=30$ and 100 nm. From Eq. (9), the normally measured feedback gain is $g_a=A_d/A_{d0}=1+E_{diss}/E_0$, so that g_a can be obtained from the E_{diss} versus z_c plotted in Fig. 4. If $F_{diss}=0$, $\Delta f(z_c)$ is independent of ϕ for each A, and from Eq. (11), this situation only changes if $E_{diss} \gg E_0$. Thus $\Delta f(z_c)$ is largely independent of ϕ in Fig. 4, although, at smaller z_c than shown, $E_{diss} \gg E_0$ and large ϕ dependences occur due to the changing Q. This strongly repulsive regime is not sampled in the present, low-Q air experiment, as it would damage the probe. For vacuum operation, with ~100 times larger Q and 100 times smaller E_0, this regime may be accessible without probe damage; Eq. (11) then yields Δf that

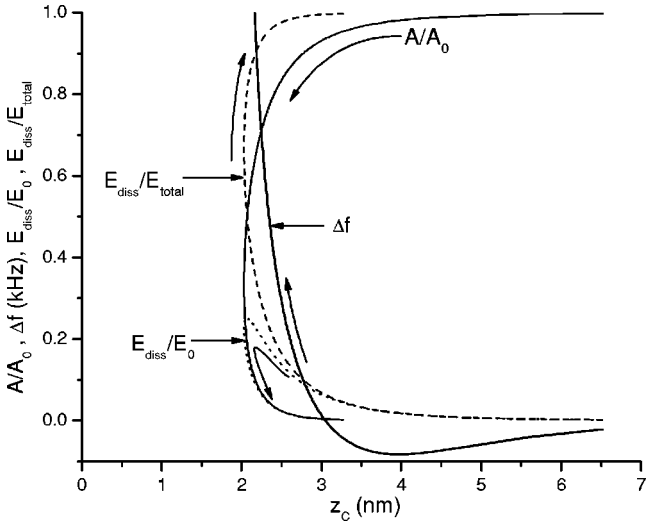

FIG. 5. Calculated frequency shift (Δf in kHz), surface-induced energy loss (E_{diss}) as a fraction of initial lever dissipation ($E_0=2500$ eV per cycle) and total (lever plus surface) dissipation (E_{total}), and oscillation amplitude (A) divided by free-lever amplitude (A_0), all as functions of the closest approach (z_c). The CE mode with $A_0=30$ nm and the sample conservative and dissipative forces described in Sec. III have been used. The arrows show the direction of response to decreasing L.

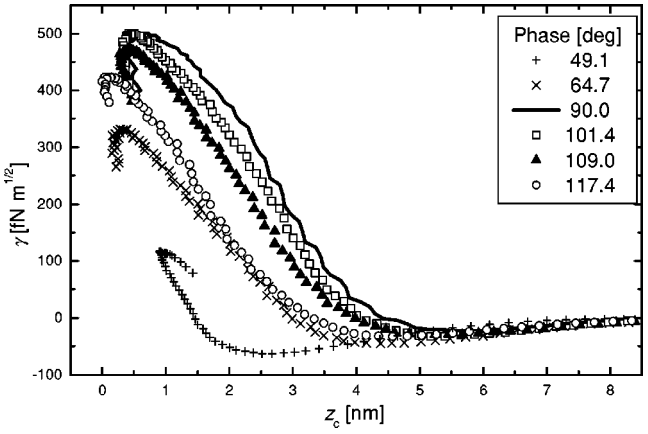

FIG. 6. Normalized frequency shift (γ) vs z_c, from the data of Fig. 2.

are sensitive to ϕ. Since the ϕ dependence of Δf is entirely due to the dissipative force, this can be used to establish $E_{diss}(z_c)$, as can A/A_d versus z_c.

To describe $f(L,A_d,\phi)$ and $A(L,A_d,\phi)$ for SO operation in CE mode, in addition to replacing z_c with $L+\Delta L-A$ in Eq. (14), A must be replaced by its dependence on A_d, ϕ and L. While this can be done, the result is neither analytic nor necessary since data can readily be reduced to $A(z_c,A_d,\phi)$ and $f(z_c,A_d,\phi)$ using the measured L, $A(L)$, and $\Delta f(L)$ to establish $z_c=L+\Delta L-A$ versus L. In essence, if SO data is reduced to a function of z_c, then either CE or CA mode can be compared to a calculation versus z_c. The primary difference is that A varies with L in the CE mode. Of course, the measurements yield changes only in z_c; the surface "contact" location is estimated only from the character of the close-range, positive $\Delta f(z_c)$, which reflects the repulsive $F_{cons}(z_c)$. To obtain A versus z_c in the CE mode for the model potentials of Eqs. (13) and (14), we take $y=A/A_0$ in Eqs. (7) and (8), where $E_{diss}(z_c,A)/E_0=y-y^2$; using $E_{diss}(z_c,A)$ from Eq. (14) yields $z_c=z_m U(A_0)^{1/(n-1.5)}$, where $U(A_0)=8Qf_0C_{diss}z_m^{3/2}n^{-1.6}/kA_0^{3/2}$. This establishes the z_c axis in Figs. 4 and 5. To emphasize that the surface energy dominates as y decreases, we have also plotted E_{diss}/E_{total} in Fig. 5, where $E_{total}=E_{diss}+E_{damp}$ is the total dissipation and $E_{damp}=y^2E_0$ is the lever dissipation.

Comparison of experimental data for $A(z_c)$ [Fig. 2(b)] with the theoretical curve (A/A_d in Fig. 5) provides reasonable agreement in the explored region (10 to 30 nm). The model F_{cons} has been adjusted to have a much larger Van der Waals attractive interaction, and a slower repulsive barrier versus z_c, than is expected between a pair H-terminated Si surfaces. That may indicate tip or surface contamination, a nonideal shape of the probe tip, or some different nonideal behavior.

E. Normalized frequency shift

The quantity $\gamma=k(\Delta f/f)A^{3/2}$, called normalized frequency shift,[5] can be used to compare approach curves at different amplitudes, to correct for amplitude and thus highlight the role of the conservative tip/sample interaction. This quantity

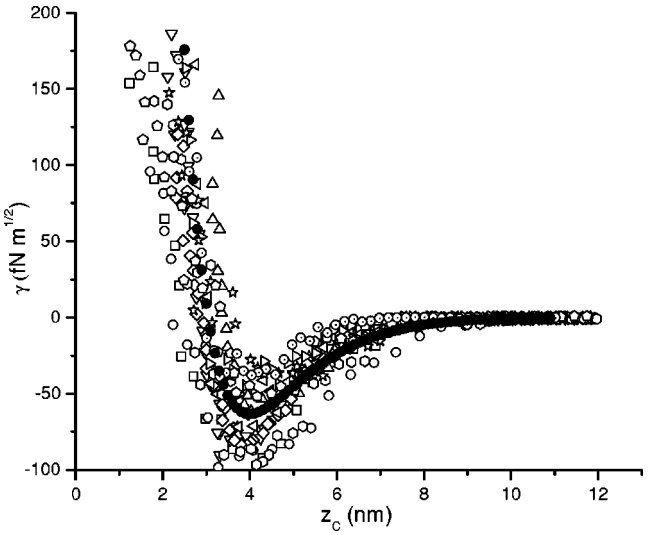

FIG. 7. Measured (open symbols) and calculated (solid points) normalized resonance frequency shift ($\gamma = k\Delta f_r A^{3/2}/f_0$), versus probe closest approach (z_c). The zero of z_c is arbitrary. Data are shown from four probes, operated at $A_0 \cong 30$ nm, that are different than the one used for Figs. 2 and 7 data.

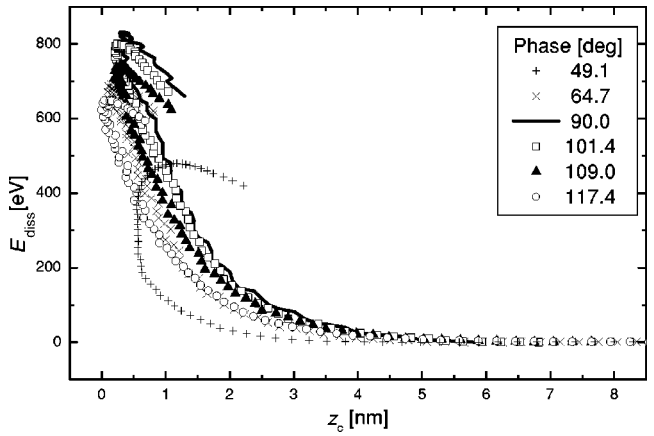

FIG. 8. Energy dissipation per cycle (E_{diss}) vs z_c, from the data of Fig. 2.

is particularly useful when operating in the CE mode, where amplitude varies within a single approach curve, as also evident from the theoretical developments of CE.[11] In Fig. 6, γ is plotted as a function of z_c, showing a negative extremum at higher separations (attractive region) followed by a maximum positive value at smaller separation in the repulsive region. The repulsive interaction is bounded in the CE mode, whereas in the CA mode it would increase monotonically with decreasing L. The two extrema are reached within a smaller separation interval for $\phi_a = \pi/2$, indicating that for such phase value higher sensitivity is obtained.

Data were taken with a variety of probes, four of which were later imaged in a TEM and found to have tip radii varying from 8 to 30 nm. Nonetheless, a relatively consistent form of attractive $\Delta f_r(z_c)$ was measured, although its magnitude and the steepness of the repulsive $\Delta f_r(z_c)$ varied by factors of >2. Some of these $\Delta f_r(z_c)$, obtained with $A \cong 30$ nm and $\phi_{set} = \pi/2$, are shown as $\gamma(z_c)$ in Fig. 7 with the minimum γ set to $z_c = 4$ nm. The theoretical $\gamma(z_c)$ is shown for comparison, as obtained from Eqs. (13) and (14).

The abrupt onset of negative Δf_r implies an abrupt onset of the conservative force, as in the $F_{cons}(z)$ given above Eq. (13). The Van der Waals and capacitive forces vary much more slowly with z, and are also much smaller than the observed force. A possible explanation of this strong, close range attraction is charge dipoles on the probe surface. Surface states within the silicon bandgap probably exist on the probe tip, and should be negatively charged in this $n+$ doped silicon. This charge is shielded within the silicon by an opposite charge distributed within the Debye length, which is ~ 1 nm in the bulk silicon but could be somewhat larger near the probe tip. We estimate that 10–30 such dipoles, interacting with the silicon substrate, could yield the observed attractive force. The repulsive interaction, associated with the positive frequency shifts at small z_c, grows relatively slowly compared to expected repulsive atomic overlaps. This type of behavior is often observed, and attributed to the presence of weakly bound adatoms on the crystal surfaces.[20] In this case of H-terminated Si, this extra attraction could be produced by hydrocarbons on the probe tip.

F. Energy dissipation

Figure 8 shows E_{diss} as a function of z_c, using Eq. (7). As expected, a maximum dissipation of $\sim\frac{1}{4}$ of the free-lever dissipation is attained at the closest range. The highest A, hence highest surface dissipation, occurs for $\phi_a = \pi/2$, where the energy dissipation per cycle is $\sim 10^3$ eV. This large value is obtained due to the high lever dissipation of our low-Q, air-operated AFM. An exponential fits well and provides a decay distance of 1.2 nm for E_{diss}. The $z_c^{-4.5}$ form in Eq. (14) provides a better fit to a variety of data with many probes, and fits the lower half of the data in Fig. 8 but is steeper than this data at small z_c. As has often been pointed out,[20] this dissipation could also be influenced by weakly bound adatoms on the crystal surfaces.

IV. CONCLUSIONS

In this paper we establish the following advancements on the understanding of SO method, and particularly of its CE mode: (i) we show full z dependence of A and Δf, and calculate conservative and dissipative surface forces, versus gap, that are consistent with the observations; (ii) we observe a minimum in the closest approach distance, in agreement with theory of CE mode extended to any phase value, and due to the double-valued relation between A and E_{diss}; and (iii) we stress the importance of accurate z control for correct quantitative DFS evaluations. We conclude that the self-oscillating, constant-excitation technique investigated here has some advantages relative to alternate methods, particularly for AFM operation in air. In essence, improvements in tip preservation, measurement reproducibility, and imaging stability can be achieved.

This work has been supported by the Quantum Physics Division of the National Institute of Standards and Technology (NIST).

*Present Address: INFM, Dipartimento di Fisica, Universita' di Pisa, Via Buonarroti 2, I-56127 Pisa, Italy

[1] G. Binnig, C.F. Quate, and C. Gerber, Phys. Rev. Lett. **56**, 930 (1986).
[2] Y. Martin, C.C. Williams, and H.K. Wickramasinghe, J. Appl. Phys. **61**, 4723 (1987).
[3] G. Meyer and N.M. Amer, Appl. Phys. Lett. **53**, 2400 (1988).
[4] Q. Zhong, D. Inniss, K. Kjoller, and V.B. Elings, Surf. Sci. Lett. **290**, 688 (1993).
[5] F.J. Giessibl, Science **267**, 68 (1995).
[6] S.N. Magonov, V. Elings, and M.-H. Whangbo, Surf. Sci. **375**, L385 (1997).
[7] J.P. Cleveland, B. Anczykowski, A.E. Schmid, and V.B. Elings, Appl. Phys. Lett. **72**, 2613 (1998).
[8] T.R. Albrecht, P. Grütter, D. Horne, and D. Rugar, J. Appl. Phys. **69**, 668 (1991).
[9] T. Uchihashi, Y. Sugawara, T. Tsukamoto, M. Ohta, S. Morita, and M. Suzuki, Phys. Rev. B **56**, 9834 (1997); H. Ueyama, Y. Sugawara, and S. Morita, Appl. Phys. A: Mater. Sci. Process. **66** (Suppl.), 295 (1998).
[10] U. Dürig, O. Züger, and A. Stalder, J. Appl. Phys. **72**, 1778 (1992).
[11] B. Gotsmann and H. Fuchs, Appl. Surf. Sci. **188**, 355 (2002).
[12] H. Hölscher, B. Gotsmann, and A. Schirmeisen, Phys. Rev. B **68**, 153401 (2003).
[13] H. Hölscher, B. Gotsmann, W. Allers, U.D. Schwarz, H. Fuchs, and R. Wiesendanger, Phys. Rev. B **64**, 075402 (2001).
[14] V.V. Protasenko, A.C. Gallagher, and D.J. Nesbitt, Proc. SPIE **4809**, 255 (2002).
[15] C. Loppacher, R. Bennewitz, O. Pfeiffer, M. Guggisberg, M. Bammerlin, S. Schär, V. Barwich, A. Baratoff, and E. Meyer, Phys. Rev. B **62**, 13 674 (2000).
[16] Y. Sugawara, M. Ohta, H. Ueyama, S. Morita, F. Osaka, S. Ohkouchi, M. Suzuki, and S. Mishima, J. Vac. Sci. Technol. B **14**, 953 (1996).
[17] M. Gauthier and M. Tsukada, Phys. Rev. Lett. **85**, 5348 (2000).
[18] B. Anczykowski, B. Gotsmann, H. Fuchs, J.P. Cleveland, and V. B. Elings, Appl. Surf. Sci. **140**, 376 (1999).
[19] B. Gotsmann, C. Seidel, B. Anczykowski, and H. Fuchs, Phys. Rev. B **60**, 11 051 (1999).
[20] See, for instance, T. Trevethan and L. Kantorovich, Nanotechnology **15**, S44 (2004).